# ON THE STATISTICAL THEORY OF UNIMOLECULAR PROCESSES

DAVID M. WARDLAW*

*Department of Chemistry, Queen's University,*
*Kingston, Ontario K7L 3N6, Canada*

R. A. MARCUS

*Arthur Amos Noyes Laboratory of Chemical Physics†,*
*California Institute of Technology,*
*Pasadena, California 91125*

## CONTENTS



* NSERC of Canada University Research Fellow.
† Contribution No. 7473.

# I. INTRODUCTION

In recent years there has been an increasing use of laser spectroscopic and other techniques to investigate unimolecular dissociations of molecules, both to initiate a dissociation and to measure the formation of the individual quantum states of the immediate reaction products. This chapter is concerned with a description of statistical theories used to calculate the rates of such dissociations, for example, of a molecule $AB$,

$$AB \rightarrow A + B, \tag{1.1}$$

and to calculate the distribution of the quantum states of the fragments $A$ and $B$. Typically, reaction rates in the literature have been calculated using RRKM theory, while distributions over various quantum states of products have been calculated mostly with phase-space theory and other models described subsequently.

Upon excitation of $AB$ with a laser pulse, the molecule may be excited to a high vibrational state of the lowest electronic state of $AB$ or to a vibrational state of an excited electronic state $AB^*$, depending on the method and on the molecule. More specifically, a wave packet of vibrational states is typically formed in each case. When the excitation is to $AB^*$, the subsequent dissociation may proceed either directly from that electronic state or, after an internal conversion, from the ground electronic state. We concentrate on the dissociation itself, and so, in the case of an internal conversion, on the behavior subsequent to the conversion.

One topic of interest is the comparison of the measured rates with those calculated using statistical theory. Commonly, the initial vibrational excitation is a nonstatistical one, as for example in the excitation of a high CH overtone of the molecule (a wave packet), which is then followed by a tendency to energy redistribution as well as by reaction. Infrared multiphoton excitation and chemical activation can be expected to be nonstatistical. If the redistribution is sufficiently rapid, the observed time decay of $AB$ in Eq. (1.1) will be a single exponential, according to statistical theory, when the energetic $AB$ has been formed with a sufficiently narrow range of energy $E$ and of angular momentum $J$, both of which affect the dissociation rate. When the redistribution is not sufficiently rapid, a more complicated time evolution for the formation of $A$ and $B$ is expected. Indeed, the assumption of a kinetic model[1] for the redistribution (involving a subdivision of the phase space into coupled subspaces) and for the reaction leads to the result that under certain conditions the long-time behavior can still be described by statistical (RRKM) theory.[2]

The study of unimolecular reactions was originally confined to thermal

studies as a function of pressure and, later, owing particularly to the pioneering work of B. S. Rabinovitch, to chemical activation studies.[3,4] In the past two or so decades a wide variety of other methods have also been introduced,[5] including the study of translational and vibrational energy distribution of products of chemical activation reactions in molecular beams, energy distributions of products of infrared multiphoton dissociation in bulk and in beams, use of high CH or OH overtone excitation to initiate unimolecular reactions, study of the angular distribution of reaction products of unimolecular reactions in molecular beams, use of picosecond techniques to study unimolecular reaction rates and quantum states of products, and the investigation of molecular ion dissociations using a variety of techniques, including coincidence measurements.

We describe several statistical approaches for calculating rates and product quantum state distributions in the following section. Illustrative applications are given in Section III, and dynamical aspects and statistical behavior are considered in a concluding Section IV.

## II. OUTLINE OF STATISTICAL THEORIES

### A. RRKM Theory

The expression for the rate constant $k_{EJ}$ for dissociation of a molecule as a function of its energy $E$ and of any other constants of the motion, such as $J$, the total angular momentum quantum number, is given in RRKM theory as[6]

$$k_{EJ} = \frac{N^{\ddagger}_{EJ}}{h\rho_{EJ}}, \tag{2.1}$$

where $N^{\ddagger}_{EJ}$ is the number of accessible quantum states of the transition state for the dissociation and $\rho_{EJ}$ is the density of states of the parent molecule at the same $E$ and $J$.

In treating isomerizations or dissociations, two limiting forms of the transition state were identified—loose and tight, or rigid, as it was termed then.[6a] In the former the separating fragments rotate freely in the transition state, while in the latter their motion is more or less similar to that in the parent molecule. In the case of reactions with a marked maximum of the potential energy along a reaction coordinate $R$, the position of the transition state $R^{\ddagger}$ was taken to occur at that $R$. In some dissociations there is little or no such maximum, and another criterion is needed for the determination of $R^{\ddagger}$. When the reactants are assumed to rotate freely at $R^{\ddagger}$, that is, when the transition state is loose, the reaction coordinate $R$ has been chosen to be the distance between the centers of mass of the separating fragments, and $R^{\ddagger}$ has then been equated, approximately, to the separation distance in a van der Waals' com-

plex of the fragments, for example, as in the Gorin model[7] described in the next section. When the orbital angular momentum (quantum number $l$) is the dominant contribution (as it frequently is) to the total angular momentum (quantum number $J$), that is, when $l \simeq J$, the orbital contribution to $N^{\ddagger}_{EJ}$ is simply $2l + 1$, that is, $2J + 1$.[4] The remaining contribution to $N^{\ddagger}_{EJ}$ is also simple, when the various remaining coordinates, apart from $R$, can be approximated by free rotations and vibrations.

The choice of the location of the transition state $R^{\ddagger}$ has been generalized by choosing it to correspond to the position of the minimum of the reactive flux along $R$ (now often called microcanonical variational transition state theory[10]). Combining this choice with a method for calculating $N^{\ddagger}_{EJ}$ for any transition state (loose, tight, or in between), Eq. (2.1) has recently been implemented for such more general systems.[11]

In the case of a loose transition state, the distribution function for the quantum states of the separated products is the same as that in the transition state, since there is no coupling between $R$ and the internal coordinates. Thus, if the number of states in the transition state that have a given quantum number $n_i$ for the $i$th coordinate is $N^{\ddagger}_{EJn_i}$ the probability $P_{EJn_i}$ that the fragments have the quantum number $n_i$ for this coordinate is

$$P_{EJn_i} = N^{\ddagger}_{EJn_i}/N^{\ddagger}_{EJ}. \tag{2.2}$$

Ideas analogous to this, together with a model for the distribution of $J$'s due to the energetic dissociating molecule being formed in a bimolecular collision, have been used to treat translational energy distributions[8] and other properties[8b] of products of bimolecular reactions involving molecular complexes as intermediates. In further work[9] we extended this type of calculation, with some added approximations, to tight transition states in the exit channel.

In general, except when the transition state is loose, the calculation of the distribution function $P_{EJn_i}$ of excess energy among the quantum states of the reaction products involves an additional approximation over and above those needed to calculate $k_{EJ}$. Examples are given in Section III.

## B. Loose Transition State and Angular Momentum Conservation (PST)

In a loose transition state there is no interaction of the radial coordinate with the internal degrees of freedom, and the reaction coordinate $R$ is chosen to be that coordinate. The effective potential $V_{\text{eff}}$ for motion along $R$ is then given (in units of $\hbar = 1$) as the sum of the actual potential and a centrifugal potential,

$$V_{\text{eff}}(R) = V(R) + \frac{l(l+1)}{2\mu R^2}, \tag{2.3}$$

where $V(R)$ is the $R$-dependent part of the potential energy and $\mu$ is the reduced mass of the separating fragments. The position of the transition state is assumed to be at the maximum of $V_{\text{eff}}(R)$,

$$\frac{\partial V_{\text{eff}}(R)}{\partial R} = 0 \quad \text{at } R = R^{\ddagger}, \tag{2.4}$$

and so this $R^{\ddagger}$ depends on $l$. Equations (2.3) and (2.4) were used in an early calculation of Gorin[7] for the recombination of methyl radicals.

If $N^{\ddagger}_{EJl}$ is the number of states for which, for the given $l$, the maximum of $V_{\text{eff}}$ is less than or equal to $E$, the $N^{\ddagger}_{EJ}$ in Eq. (2.1) equals

$$N^{\ddagger}_{EJ} = \sum_{l} N^{\ddagger}_{EJl}. \tag{2.5}$$

If the approximation $l \simeq J$ is introduced, the sum in (2.5) consists only of one term.

We consider next phase-space theory (PST), which was designed principally to calculate energy distributions of the reaction products.[12] In PST a loose transition state is assumed and, rather than using the approximation of $l \simeq J$, $l$ is chosen so as to satisfy angular momentum conservation, namely, the triangle inequality,

$$|J - k| \leq l \leq J + k, \tag{2.6}$$

where $k$ is an integer, a quantum number, corresponding to the vector sum of the rotational angular momenta of the two fragments (quantum numbers $j_1$ and $j_2$); $k$, itself, satisfies the triangle inequality

$$|j_1 - j_2| \leq k \leq j_1 + j_2. \tag{2.7}$$

The various states contributing to $N^{\ddagger}_{EJ}$ contain as quantum numbers $J$, $l$, $j_1$, $j_2$, $k$, $\kappa_1$, $\kappa_2$, together with the vibrational quantum numbers of each fragment. Here, $\kappa_i$ is the quantum number which, in addition to $j_i$ ($i = 1, 2$), specifies the rotational energy of fragment $i$. (There are $2j_i + 1$ values of $\kappa_i$, for any $j_i$. If fragment $i$ is a symmetric top, $\kappa_i$ is the component of $j_i$ along the symmetry axis.) The absence of coupling terms between the radial motion $R$ and the remaining coordinates in Eq. (2.3) reflects the fact that the separating fragments rotate freely in a loose transition state. The calculation of each $N^{\ddagger}_{EJl}$ is relatively straightforward albeit numerical because of the constraints (2.6) and (2.7). The quantity of major interest in applications of PST is the distribution function $P_{EJn_l}$, which is given by Eq. (2.2).

The assumption of a loose transition state provides only an upper bound

to the dissociation rate constant, apart from possible tunneling effects, which are usually quite minor for dissociations into polyatomic fragments. Frequently, the $R$-motion in the exit channel is coupled to the other coordinates, for example to the developing rotations of the fragments, and the latter are coupled to each other, resulting in a hindered rather than free rotational motion of the separating fragments in the transition state. The resulting quantum states contributing to $N_{EJ}^{\ddagger}$ in Eq. (2.1) are then more widely spaced than when the fragments rotate freely, and so the states are fewer in number. The actual $k_{EJ}$ is then less than the PST value, a result well known for many reactions.[13]

Again, in the case of a dissociation reaction in which the transition state was not loose (e.g., the reverse reaction of methyl radical addition to an olefin had a steric factor), PST did not adequately describe the translational energy distribution of the products, and resort was made to a more general treatment that made some allowance for hindered motions.[9]

We turn in the next section to a recent treatment that allows for these coupled hindered rotational motions.[11]

### C. General Transition State and Angular Momentum Conservation (RRKM)

We consider here the implementation of Eq. (2.1) for more general transition states. When the transition state is loose, it occurs at the maximum in $V_{\text{eff}}$, as in Eq. (2.4). However, when the rotational motion of the separating fragments is hindered, owing to their coupled behavior, a more general criterion for $R^{\ddagger}$ is needed. Often in dissociations into free radicals there is no appreciable potential energy maximum to suggest an $R^{\ddagger}$, and the criterion (2.4) is also clearly inadequate for the more general case. An appropriate criterion arises from Wigner's and Keck's classical version of variational transition state theory,[14] where the transition state, a hypersurface in phase space now, is chosen so as to have the minimum flux from reactants to products passing through it. In this case, there are the fewest recrossings of the transition state hypersurface by classical trajectories and the transition state calculated rate becomes an increasingly better bound to the actual rate.[14b]

When the motion along the reaction coordinate is treated classically and the remaining coordinates quantum mechanically, it is convenient to define $N_{EJ}(R)$, the number of states with energy equal to or less than $E$ for the given $J$ and for that $R$. The flux along $R$ at any point $R$ is proportional to $N_{EJ}(R)$, as can be seen, for example, from Eq. (2.1), since $k_{EJ}$ is proportional to the flux. Thus, the location $R^{\ddagger}$ of the transition state along $R$ (loose, tight, or in between) is determined as the $R$ that minimizes $N_{EJ}(R)$:[10]

$$\frac{\partial N_{EJ}(R)}{\partial R} = 0 \quad \text{at} \quad R = R^{\ddagger}. \tag{2.8}$$

Recently, we described a method for implementing Eq. (2.1) using (2.8) in a way in which $N_{EJ}(R)$ is calculated so as to satisfy the angular momentum triangle inequalities (2.6) and (2.7) for any prescribed potential energy function in the exit channel.[11] There is at least one price to pay for this generalization: While the expression for $N^{\ddagger}_{EJ}$ in the case of a tight transition state, or in the case of a loose transition state with $l \simeq J$, was evaluated analytically,[6] the expression in this more general implementation of Eq. (2.1) is evaluated numerically. In applications to dissociations thus far, we have chosen the reaction coordinate $R$ to be the distance between the centers of mass of the separating fragments.

The complexity of evaluating $N_{EJ}(R)$ and, by its minimization $N^{\ddagger}_{EJ}$, in the case of transition states that are neither loose nor tight, arises because of the coupled bending and rotational motion of the parent molecule, motions that become free rotations and orbital motion of the separated fragments.[11] A quantum calculation of the energy eigenvalues of these typically six or so coordinates (termed "transitional coordinates") at each $R$, for the given potential energy surface, would permit the determination of all such states contributing to $N_{EJ}(R)$, for the given $E$ and $J$. When these states of the transitional coordinates are convoluted with $N_v$, the number of states from the more simply treated remaining coordinates, the total number of states $N_{EJ}(R)$ would then be obtained.

We have adopted the following procedure.[11] $N_{EJ}(R)$ is written as a convolution for each $R$,

$$N_{EJ}(R) = \int_0^E N_v(E - \varepsilon)\Omega_J(\varepsilon)\, d\varepsilon, \tag{2.9}$$

where $\Omega_J(\varepsilon)$ is the density of states of the "transitional" (coupled bending vibrational–rotational) degrees of freedom in the energy interval $(\varepsilon, \varepsilon + d\varepsilon)$, and $N_v(E - \varepsilon)$ is the number of quantum states for the coordinates not present in $\Omega_J$, when their energy is equal to or less than $E - \varepsilon$. The two types of coordinates are taken to be uncoupled from each other, apart from their dependence on $R$. The value of $N_v$ in Eq. (2.9) is obtained by the usual quantum count. The main approximation is in the evaluation of $\Omega_J(\varepsilon)$.

We have found it convenient to calculate $\Omega_J(\varepsilon)$ classically and to express the coordinates contributing to $\Omega_J(\varepsilon)$ in terms of action-angle variables. (Approximate quantum corrections can be made.[11]) The actions are the classical counterparts of the quantum numbers $j_1$, $j_2$, $\kappa_1$, $\kappa_2$, $k$, $l$, and $J$ previously mentioned, and we shall simply denote the actions by the same symbols to simplify the notation. When the $i$th fragment is an atom the numbers $j_i$, $\kappa_i$ and $k$ are absent, while if one of the fragments is a linear molecule, its $\kappa_i$ is absent. For two nonlinear fragments we have, in units of $\hbar = 1$,[11] for a

particular electronic state, and apart from any electronic multiplicity factor,

$$N_{EJ}(R) = (2J + 1)(2\pi)^{-6}\sigma^{-1} \times \int \cdots \int N_V(E - H_{cl})\Delta(J,k,l)\Delta(k,j_1,j_2)\, dj_1\, dj_2\, d\kappa_1\, d\kappa_2\, dk\, dl\, d\alpha, \tag{2.10}$$

where $d\alpha$ is the volume element for the angle variables conjugate to the six action integration variables in Eq. (2.10). The $\sigma$ denotes the symmetry number for transformations involving these six angle coordinates.[6] Each angle is integrated over the interval 0 to $2\pi$, within the limits imposed by energy conservation. The action variables are restricted both by energy conservation and by the triangle inequalities (2.6) and (2.7), each $\Delta$ being unity when the relevant inequality is fulfilled and zero otherwise. Each $\kappa_i$ is restricted by the condition $|\kappa_i| \leq j_i$. (In practice, a symmetric top approximation will be typically used for fragment $i$, and then $\kappa_i$ refers to the component of $j_i$ along the symmetry axis.) $H_{cl}$ is the part of the Hamiltonian that refers to the coordinates contributing to $\Omega_J(\varepsilon)$, for example, as in Eq. (II.2) of Ref. 11c. Equations (2.1) and (2.8)–(2.10) are used for the calculation of the rate constants $k_{EJ}$, the integral in (2.10) being evaluated by a Monte Carlo method. The calculation of the thermally averaged value of $k_{EJ}$ is given later.

A calculation of the distribution function $P_{EJn_i}$ for the quantum states of the reaction products requires an additional approximation over and above that needed for $k_{EJ}$. One approximation is to assume an adiabaticity in the exit channel, wherein the lowest states in $N^{\ddagger}_{EJ}$ correlate adiabatically with the lowest states in the products.[2] The relative probability $P_{EJn_i}$ that the quantum state of the $i$th coordinate is $n_i$ is then given by[2]

$$P_{EJn_i} = N^{\infty}_{E'-E_i,J}/N^{\ddagger}_{EJ}, \tag{2.11}$$

where $E'$ is defined by the condition

$$N^{\ddagger}_{EJ} = N^{\infty}_{E'J}, \tag{2.12}$$

$N^{\infty}_{E'J}$ being the number of quantum states of the products at $R = \infty$ with energy less than or equal to $E'$, $N^{\infty}_{E'-E_i,J}$ is the corresponding number at $R = \infty$ when there is an energy $E_i$ in the $i$th coordinate (or set of coordinates) of the products and the quantum number for this coordinate (or totality of quantum numbers) is $n_i$. When states of different symmetry are involved along the entire reaction coordinate, a suitable classification of the states in (2.11) by symmetry is first made. A variant of (2.11) assumes that $l$ is a constant in the exit channel; this

variant reduces to PST in the limit that the hindered rotations at $R^{\ddagger}$ become free.[2] However, when $l \simeq J$, $l$ becomes essentially a constant of the motion automatically, and so even Eqs. (2.11)–(2.12) reduce approximately to PST in the limit that the rotations at $R^{\ddagger}$ are free. Otherwise, Eqs. (2.11)–(2.12) reduce to PST only on the average in the free rotation limit.

### D. Vibrationally Adiabatic Transition State and SACM

Adiabatic, or as it has been termed vibrationally adiabatic,[15] transition state theory has its origin in a paragraph in an article by Hirschfelder and Wigner.[16] The treatment was developed further by a number of authors.[17] In this type of transition state theory the eigenvalues of the system at each $R$, which are the vibrationally adiabatic eigenvalues, are plotted versus $R$. The $N_{EJ}^{\ddagger}$ in Eq. (2.1) then becomes the number of such states whose maximum energy on this plot does not exceed $E$, that is, $N_{EJ}^{\ddagger}$ now denotes the sum of all open adiabatic reaction channels.

In principle, this $N_{EJ}^{\ddagger}$ can be determined if the potential energy surface is known: For the given $J$ value and for each value of the reaction coordinate $R$ (e.g., the bond length of the dissociating bond or the distance between the centers of mass of the two separating fragments), the vibrational–rotational quantum eigenvalues $E_v(R)$ are obtained. The result is a set of nonintersecting adiabatic channel curves that smoothly connect, and hence correlate, the reactant (parent molecule) and product (separated fragments) vibrational–rotational energy levels. Each curve $E_v(R)$ has a maximum $E_{max}$ at some $R$ in the exit channel. $N_{EJ}^{\ddagger}$ is then the sum of all open adiabatic channel curves, that is, those curves for which $E_{max} < E$. In practice, the full potential energy functions are usually unavailable and, even if they were, obtaining the quantum eigenvalues (perhaps by matrix diagonalization) at all relevant values of $R$ is simply not practical at present for most systems. The intermediate region between reactants ($R = R_e$) and products ($R = \infty$) presents the greatest computational difficulties for both the potential energy function and the eigenvalues, and this region often determines the reaction rate of the bond fission process.

The model of Quack and Troe,[18] the statistical adiabatic channel model (SACM), is an approximate prescription for calculating the number of open adiabatic channels. A universal function $g(R)$ is assumed for interpolating between all eigenvalues of reactants and products,[19]

$$g(R) = \exp[-\alpha(R - R_e)], \tag{2.13}$$

with $\alpha$ being treated as an adjustable parameter. In fitting SACM to thermal rate data, typically $\alpha \sim 1$ Å$^{-1}$.[20] Even with this approximation, as indicated in the original presentation[18] of SACM, direct numerical count for $N_{EJ}^{\ddagger}$

becomes exceedingly time consuming for large molecules, owing to the large number of reactant and product energy levels to be correlated and the correspondingly large number of channel maxima to be located (usually numerically). Various additional approximations have been postulated to simplify the calculation.[21]

The distribution (relative probability) of products having a quantum number $n_i$ for mode $i$ is again given by Eq. (2.2), where $N^{\ddagger}_{EJn_i}$ now denotes the number of open adiabatic channels leading to products in state $n_i$ and $N^{\ddagger}_{EJ}$ is the total number of open adiabatic channels at the given $E$ and $J$.[22]

## III. APPLICATIONS

In this section several recent applications of the methods previously described are summarized for some selected bond fissions or for the reverse reactions. No attempt is made to provide a comprehensive review of all such applications. Applications to ion–molecule reactions[23,24] have also been omitted. Some specialized statistical models have been developed[23] for this topic.

### A. $CH_3$ Recombination

The recombination of methyl radicals to form ethane

$$2CH_3 \xrightarrow{k_r} C_2H_6 \tag{3.1}$$

has been widely studied experimentally under various conditions, the recombination rate constant $k_r$ being defined by

$$-\frac{d[CH_3]}{dt} = 2k_r[CH_3]^2. \tag{3.2}$$

Many statistical models have been applied to reaction (3.1), and it might be considered a test case for theoretical treatments of the rate constant. The process inverse to (3.1), the dissociation of ethane, has also been extensively studied experimentally[25,26] and theoretically.[11b,22,27] The theoretical predictions for the rate of dissociation are, of course, quite sensitive to the value of the bond dissociation energy. On the other hand, recombination rates depend only weakly on that quantity. In the present review, attention is focused on the prediction of the recombination rate using the transition state theory outlined in Section II C. First, the high-pressure limit of $k_r$, denoted by $k_\infty$, is considered, particularly its temperature dependence. This is followed by a brief description of some results for the pressure dependence of $k_r$ and for the dissociation of a vibrationally excited $C_2H_6$ molecule.

### 1. *High-Pressure Rate*

In the following the salient features of the general transition state theory of Sections II A and II C, as applied to methyl radical recombination, are summarized. Details, where omitted, are given in Ref. 11*c*.

The high-pressure recombination rate constant $k_\infty$ is given as a function of the temperature $T$ by[28]

$$k_\infty(T) = \frac{g_e}{hQ_r(T)} \int_0^\infty dE \sum_{J=0}^{\infty} (2J+1) N_{EJ}(R^\ddagger) e^{-E/kT}, \tag{3.3}$$

where $E$ is the total energy in the center-of-mass frame, $J$ and $N_{EJ}(R)$ were defined earlier, and $R^\ddagger$ was defined by Eq. (2.8); $Q_r$ is the partition function, in the center-of-mass frame, for the pair of reactants at infinite separation and is evaluated in a standard fashion[29]; $g_e$ is the ratio $g^\ddagger/g_1g_2$ of electronic partition functions for the transition state and separated radicals and is taken to be $\frac{1}{4}$, corresponding to a common situation that only systems initially on the singlet potential energy surface lead to recombination products.

The main ideas in the calculation of $N_{EJ}$ were described earlier (Section II C). For the specific case of reaction (3.1), Eq. (2.10) is used for $N_{EJ}(R)$. The classical Hamiltonian $H_{cl}$ in (2.10) is written as

$$H_{cl} = \sum_{i=1,2} E_{ri} + \frac{l^2}{2\mu R^2} + V_t(r_{mn}, \theta_1, \theta_2), \tag{3.4}$$

where $E_{ri}$ is the rotational energy obtained from a rigid oblate symmetric top model of methyl radical $i (i = 1, 2)$ with $R$-dependent moments of inertia; $\mu$ is the reduced mass for relative motion of the two fragments; $V_t$ is the potential energy function for the transitional modes (specifically, for variation in the separation distance and in the orientation of the $CH_3$ groups); $r_{mn}$ denotes a $4 \times 4$ set of interfragment distances between atom $n (n = 1$ to 4) of fragment 1 and atom $m (m = 1$ to 4) of fragment 2; $\theta_i$ is the angle between the carbon–carbon displacement vector $\mathbf{r}_{CC} \equiv \mathbf{r}_{44}$ and the symmetry axis of methyl radical $i (i = 1, 2)$. The internal coordinates $r_{mn}, \theta_1, \theta_2$ that determine $V_t$ in Eq. (3.4) are completely specified (using a transformation given in Ref. 11*c*) by $R$, $J$ and the 12 variables of integration in Eq. (2.10). The $l$ in Eq. (3.4) denotes an action, the orbital angular momentum $l_{cl}$, and is related semiclassically to the quantum number $l$ in Eq. (2.3) by $l_{cl} \approx (l + \frac{1}{2})$ (in units of $\hbar = 1$) and so the $l^2$ in Eq. (3.4) denotes $l_{cl}^2$, that is, $(l + \frac{1}{2})^2$, which is the semiclassical (Langer) approximation to the $l(l + 1)$ in Eq. (2.3). The potential $V_t$ is intended to be physically reasonable, and can be constructed from *ab initio* points when they become available. It is to be emphasized that the present method can be used

regardless of the explicit form of the potential energy surface for the transitional modes (or for the conserved modes) and regardless of whether or not $l$ is a constant of the motion.

The transitional mode potential was assumed to arise from nonbonded and bonded interactions

$$V_t = V_{NB} + V_B, \tag{3.5}$$

where $V_{NB}$ is a sum of Lennard-Jones potentials between all nonbonded C···H and H···H pairs and $V_B$ is a Morse function modified by an orientational factor to include in an approximate way to the now bent C···C bond. The explicit forms of $V_{NB}$ and $V_B$ are given in Ref. 11*c*.

In the absence of a current precise knowledge of the potential energy surface, interpolations were used to obtain approximate normal mode frequencies for the conserved modes and methyl radical moments of inertia at intermediate $R$ values, as described in Ref. 11*c*, using the interpolation $g(R)$ specified by Eq. (2.13). The number of quantum states for the conserved modes [$N_V$ in Eq. (2.10)] was obtained at each value of $R$ by a direct count of the approximately harmonic levels. Calculations were made for two values of $\alpha$ in Ref. 11*c*, as reported below. The potential energy and structural parameters that determine $V_t$, the conserved mode frequencies, and the moments of inertia are given in tables in Ref. 11*c*.

Three related approaches to the calculation of the recombination rate constant are described subsequently, the second two being approximations to the first. In each case the integral over $E$ and the sum over $J$ in the numerator of Eq. (3.3) are approximated by $N$-point Laguerre and $2M$-point extended Simpson's rule quadratures,[30] respectively, yielding

$$k_\infty^I(T) = \frac{g_e kT}{hQ_r(T)} \frac{\Delta J}{3} \sum_{i=1}^{N} \sum_{j=0}^{2M} w_i w_j N_{E_i J_j}(R_I^\ddagger), \tag{3.6}$$

where $E_i = kTx_i$, $w_i$ and $x_i$ are Laguerre weights and points,[30] $\Delta J$ is the constant step size for the $J$-quadature, $J_j = j\Delta J$, with $j$ being an integer, not to be confused with the $j_i$'s in Eq. (2.10), and $w_j = 1$ for $j = 0$ and $2M$, $w_j = 2$ for $j$ even $w_j = 4$ for $j$ odd.

The transition state location $R_I^\ddagger$ was determined for each $(E_i, J_j)$ pair in Eq. (3.6) by minimizing $N_{E_i J_j}$ with respect to $R$ on a 0.1 Å grid over an appropriate range of $R$ values. The variation in $R_I^\ddagger$ with energy is depicted in Fig. 1 for several of the $J$ values employed in the evaluation of Eq. (3.6). The integral appearing in the expression for $N_{EJ}(R)$ in Eq. (2.10) was evaluated by the Monte Carlo method described in Ref. 11*b* and is not discussed here. The Monte Carlo approximation to $N_{EJ}(R)$ was denoted by $N_{EJ} \pm \sigma^{MC}$, where $\sigma^{MC}$

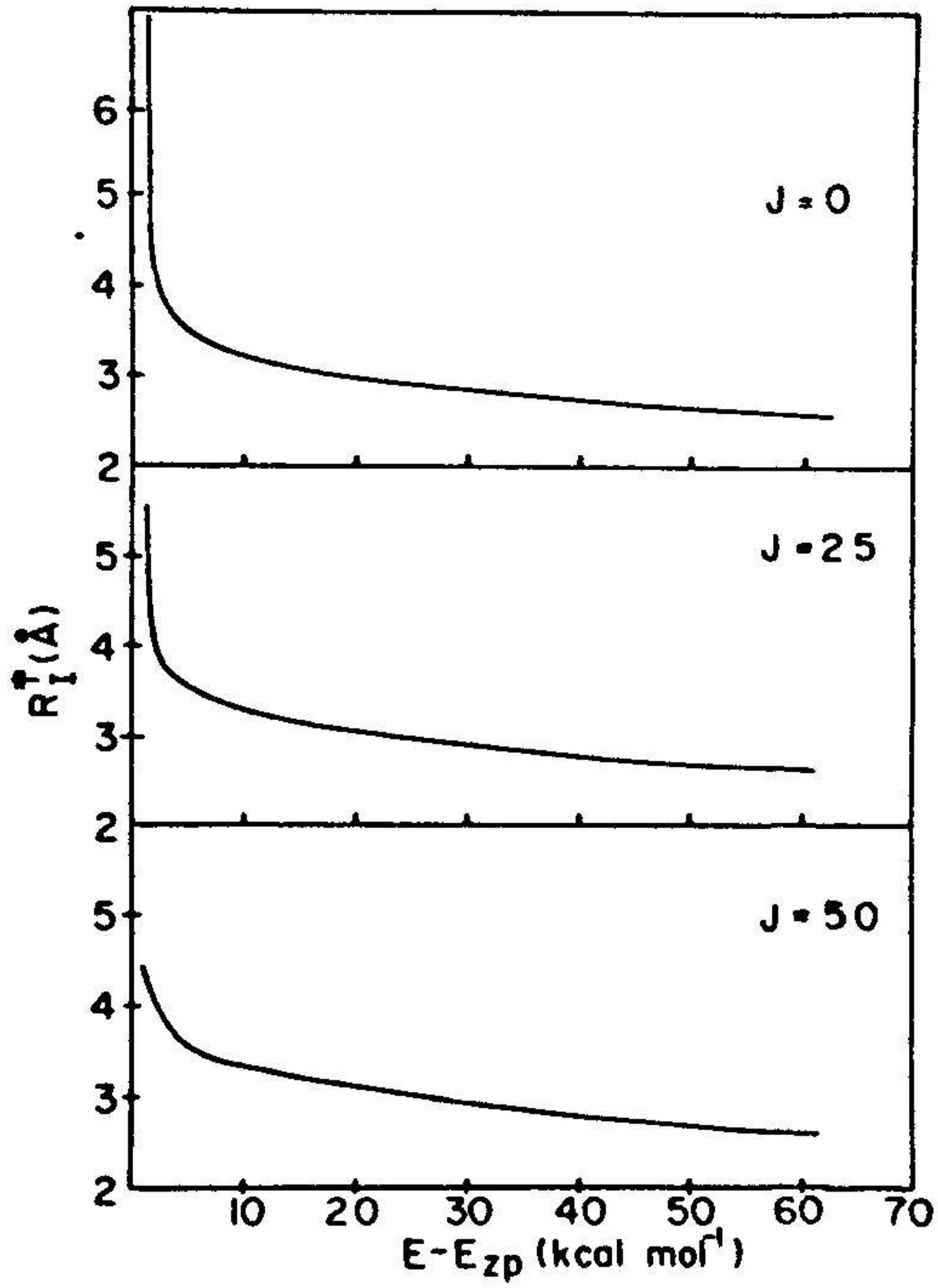


**Figure 1.** Plot of the transition state location versus the energy in excess of the total zero-point energy of separated methyl radicals for several values of the total angular momentum $J$. The solid curves result from smoothly connecting $R_I^{\ddagger}$ values for discrete values of the energy $E$. Each $R_I^{\ddagger}$ was obtained for a particular $(E, J)$ pair by minimizing $N_{E,J}$ with respect to $R$ on a 0.1 Å grid over an appropriate range of $R$ values.

is one standard deviation. Estimates of the upper and lower bounds on $k_\infty^I(T)$ were obtained by using $(N_{E_i J_j} + \sigma^{MC})$ and $(N_{E_i J_j} - \sigma^{MC})$, respectively, in Eq. (3.6). Convergence of the quadratures in Eq. (3.6) was ascertained by the agreement (within upper and lower bounds) of $k_\infty^I$ values obtained with different values of $N$ and $2M$.[11c] Since the model potential $V_t$ for the transitional modes admits, for sufficiently small values of $R$ and $E$, disjoint regions of energetically accessible classical phase space, an *ad hoc* restriction in the Monte Carlo sampling procedure was introduced[11c] to account for this feature.

The symmetry factor $\sigma$ in Eq. (2.10) deserves special consideration. A loose transition state will be characterized by large values of $R_I^{\ddagger}$ and, hence, will have essentially planar methyl radicals. In this case each of the identical fragments has both $C_{2v}$ and $C_{3v}$ axes, resulting in a $\sigma = (3 \times 2)^2 \times 2 = 72$. The results given in Table I were obtained using this value of $\sigma$. Results obtained by an

TABLE I
High-Pressure Recombination Rate Constants[a]

| Temperature (K) | Rate Constants ($10^{13}$ cm$^3$ mol$^{-1}$ sec$^{-1}$) | | |
|---|---|---|---|
| | $k_\infty^I \pm \delta^I$ | $k_\infty^{II} + \delta^{II}$ | $k_\infty^{III} \pm \delta^{III}$ |
| 300 | 4.33 ± 0.12 | 4.28 ± 0.10 | 5.08 ± 0.13 |
| 500 | 3.67 ± 0.08 | 3.58 ± 0.08 | 4.38 ± 0.06 |
| 1000 | 2.37 ± 0.06 | 2.29 ± 0.06 | 2.79 ± 0.06 |
| 2000 | 1.09 ± 0.04 | 1.08 ± 0.03 | 1.32 ± 0.03 |

[a] All rate constants calculated with a value of 1.0 Å$^{-1}$ for the potential energy surface interpolation parameter $\alpha$; $k_\infty^I = \frac{1}{2}[(k_\infty^I)_{max} + (k_\infty^I)_{min}]$ and $\delta = \frac{1}{2}[(k_\infty^I)_{max} - (k_\infty^I)_{min}]$, where $(k_\infty^I)_{max}$ and $(k_\infty^I)_{min}$ are estimated upper and lower bounds obtained by using $N_{E,J_i} + \sigma^{MC}$ and $N_{E,J_i} - \sigma^{MC}$, respectively, in Eq. (3.6); analogous expressions define $(k_\infty^{II}, \delta^{II})$ and $(k_\infty^{III}, \delta^{III})$.

approximate interpolation taking into account the umbrella shape of the methyl radicals at smaller $R$ values are also reported in Ref. 11c and are discussed briefly here. Motivation for use of an $R$-dependent symmetry correction is provided by Fig. 1 in which the decrease in $R_J^\ddagger$ with increasing $E$ is evident.

In the process of evaluating $k_\infty^I$ in Eq. (3.6) it was found[11c] that $R_J^\ddagger$ was approximately independent of $J$ for a given $E$. Accordingly, as an approximation to $k_\infty^I$, a quantity $k_\infty^{II}$ was introduced as follows: A $J$-averaged $N_{EJ}(R)$ was first defined, for use in (3.3),

$$N_E(R) = \int_0^{J_{max}} dJ\, N_{EJ}(R), \tag{3.7}$$

where $J_{max}$ is the maximum $J$ for a rigid symmetric top model of $C_2H_6$ when all of the available energy appears as overall rotation of the $C_2H_6$. The integral over $E$ in Eq. (3.3) was then replaced by an $N$-point Laguerre quadrature, as for $k_\infty^I$, and the resulting approximation to Eq. (3.3) became

$$k_\infty^{II}(T) = \frac{g_e kT}{hQ_r(T)} \sum_{i=1}^{N} w_i N_{E_i}(R_{II}^\ddagger). \tag{3.8}$$

In constrast with $k_\infty^I$ the transition state location $R_{II}^\ddagger$ is now determined for each $E_i$ in Eq. (3.8) by minimizing $N_{E_i}$ with respect to $R$ on a 0.1 Å grid. The integral for $N_E(R)$ in Eq. (3.7) was evaluated by extending the Monte Carlo method described in Ref. 11b to include the additional integration over $J$. $k_\infty^{II}(T)$ will equal $k_\infty^I(T)$ when $R_J^\ddagger$ is independent of $J$. The advantage of using Eq. (3.8) instead of Eq. (3.6) lies in the elimination of individual Monte Carlo calculations for each of the discrete $J_j$'s in Eq. (3.6) and a concomittant 3–5-fold

reduction in the total number of required Monte Carlo points; the precise reduction factor varied with temperature. Agreement of the $k_\infty^I$ and $k_\infty^{II}$ values was found[11c] for the particular model of methyl radical recombination under consideration.

In a third approach, a canonical rate constant, denoted by $k_\infty^{III}$, was obtained in order to assess the error introduced by neglecting the dependence of the transition state location on $E$ and $J$. This rate constant $k_\infty^{III}$ is given by

$$k_\infty^{III}(T) = \frac{g_e kT}{hQ_r(T)} \sum_{i=1}^{N} w_i N_{E_i}, \tag{3.9}$$

where the sum is evaluated at the transition state location $R_{III}^\ddagger$, which is determined by minimizing that sum with respect to $R$ on a 0.2 Å grid; this value of $R_{III}^\ddagger$ is thereby independent of $E_i$. The evaluation of $N_{E_i}$ in Eq. (3.9) is as described above. $k_\infty^{III}$ equals $k_\infty^I$ when $R_I^\ddagger$ is independent of both $E$ and $J$. The procedure of using $k_\infty^{III}$ [though not using Eqs. (2.10) and (3.7) specifically] has often been employed in some of the earlier literature on reaction rates, where the procedure is referred to as a maximization of free energy of activation and, more recently, as canonical variational transition state theory.

Results for $k_\infty^I$, $k_\infty^{II}$, and $k_\infty^{III}$ are given in Table I for the temperatures 300, 500, 1000, and 2000 K, which approximately span the temperature range studied in the collective experimental work on the high-pressure limit of the methyl radical recombination rate. All results in Table I were obtained with $\alpha = 1$ Å$^{-1}$ [Eq. (2.13)]. The $k_\infty^I$ and $k_\infty^{II}$ values are seen to agree, within the numerical uncertainty (denoted by $\delta$ in Table I), for the four temperatures studied. The canonical rate constant $k_\infty^{III}$ is seen to be greater than $k_\infty^I$ or $k_\infty^{II}$ by about 20% at each temperature. Since at each $R$, $N_{EJ}(R) \geq N_{EJ}(R_I^\ddagger)$, $k_\infty^{III}$ should indeed be an upper bound to $k_\infty^I$. For the Monte Carlo method in Ref. 11c the computational effort used to obtain $k_\infty^{III}$ via the energy quadrature in Eq. (3.9) was approximately the same as that for the preferred $k_\infty^{II}$ [Eq. (3.8)]. (An attempt to include the energy integral in the most straightforward way in the Monte Carlo procedure in Ref. 11c substantially increased the required computer time. However, an improved weighting factor for the Monte Carlo sampling may be available.)

Of particular interest both theoretically and experimentally is the temperature dependence of $k_\infty$. Much of the available experimental data on $k_\infty$ is displayed in Fig. 2 of Ref. 11c. These data span the temperature range 250–2500 K and were published over a period from 1951 to 1985. A comprehensive review of pre-1980 experimental work on methyl radical recombination has been published by Baulch and Duxbury.[26] The large scatter in the data is evident in Fig. 2 of Ref. 11c and some of the experimental uncertainties (not shown in that figure) are large. Nevertheless, it appears that $k_\infty$ may exhibit

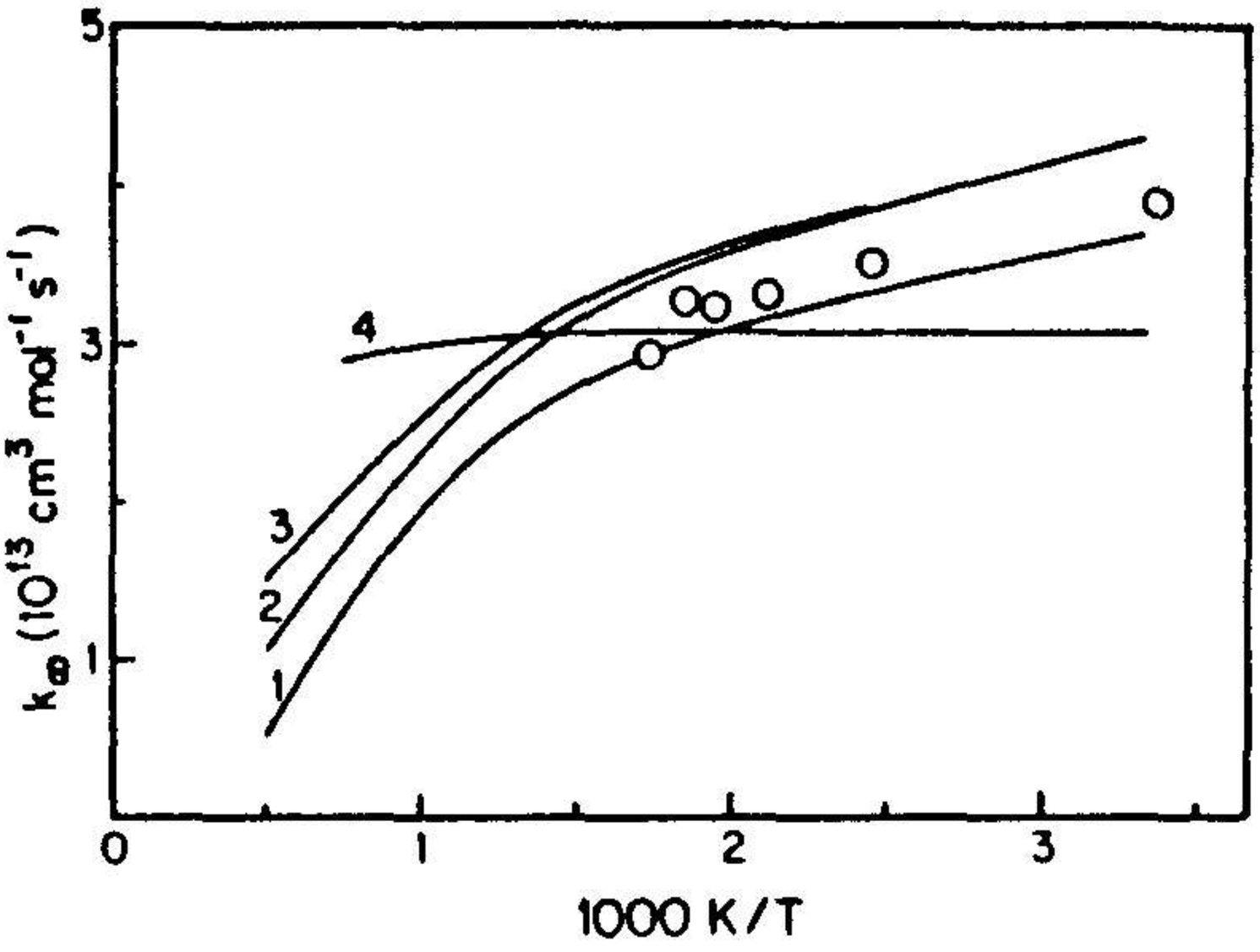


**Figure 2.** Plot of the high-pressure rate constant for $CH_3$ recombination versus reciprocal temperature. Theoretical results are presented as solid curves 1 through 4 and are discussed in the text: (1) generalized RRKM with $\alpha = 0.8$ Å$^{-1}$; (2) generalized RRKM with $\alpha = 1$ Å$^{-1}$; (3) generalized RRKM with $\alpha = 1$ Å$^{-1}$ and an approximate symmetry correction; (4) a simplified SACM treatment. The open circles are the experimental results of Ref. 33.

a negative temperature dependence, that is, a decrease in $k_\infty$ with increasing temperature. In their survey Olson and Gardiner[25] judged that "the consensus value of the recombination rate constant near 1000 K is seen to be a factor of 3 lower than the room-temperature consensus value." The present theoretical calculation yielded a similar result.[11c] However, accurate experimental determinations of $k_\infty$ require an extrapolation of results at various pressures, yielding some uncertainty in the quantitative temperature dependence, particularly at high temperatures, where a large extrapolation was needed.

Some of the present flexible transition state theory results for methyl radical recombination are given in Fig. 2, a plot of $k_\infty$ versus 1/T. Curves 1 and 2 depict $k_\infty^{II}$ for $\alpha = 0.8$ and 1 Å$^{-1}$, respectively,[31] curve 3 depicts the results, denoted by $k_\infty^{II'}$, of a $k_\infty^{II}$ calculation with $\alpha = 1$ Å$^{-1}$ in which the anticipated deviation of the symmetry number from its loose value was included in an approximate way.[11c] Each curve was obtained by smoothly connecting the calculated values of $k_\infty^r$ at $T = 300$, 500, 1000, and 2000 K. Plots of $k_\infty^{II}$, rather than the correct $k_\infty^I$, were presented because the $k_\infty^{II}$ calculations involved significantly less computation time and yielded results in close numerical agreement with those of the corresponding $k_\infty^I$ calculations. As might have been expected, the rate constant decreased when $\alpha$ was decreased from 1 to 0.8 Å$^{-1}$, in this case the decrease being about 10% at all four temperatures studied. At $T = 300$ K, $k_\infty^{II'}$ (curve 3) agrees with $k_\infty^{II}$ (curve 2) but does not decrease as rapidly with increasing $T$ and is about 40% greater than $k_\infty^{II}$ at $T \sim 2000$ K. In terms of the present model, the trend of decreasing $k_\infty$ with

increasing $T$ is attributable to the decrease in $R^{\ddagger}$ with the increasing available energy $E$ associated with increasing temperature (Fig. 1). As the transition state becomes tighter deviations from a loose symmetry number become more pronounced.

A noteworthy feature of all three curves in Fig. 2 is the distinct negative temperature dependence. A number of other statistical models have been used to obtain $k_\infty$ values for this system. Many of these results are displayed in Fig. 2 of Ref. 11*c* and are discussed in the text accompanying that figure. Only two other models displaying a negative temperature dependence have been reported: a simplified SACM treatment[18] displayed a very small negative temperature dependence (curve 4 in Fig. 2). For a Gorin model loose transition state, modified by the *ad hoc* inclusion of geometrically derived steric factors for each radical (not given in Fig. 2), qualitative considerations indicated a rough estimate of $T^{-1/6}$ for the temperature dependence of $k_\infty$.[32]

Comparison with experiment in the present Fig. 2 is given for the 1985 results of Macpherson et al.[33] whose data appear as open circles. There is agreement with the general transition state theory calculations over the experimentally studied temperature range 296–577 K for curve 1. A feature of the data in Ref. 33 is the accurate determination of the absorption cross section $\sigma_a$ for the $CH_3$ absorption at 216.36 nm. This determination was important since most experimental studies of the $CH_3$ recombination rate accurately measure the ratio $k_\infty/\sigma_a$. In many earlier determinations of $k_\infty$, one source of error appears to lie in the absorption cross section, a case in point being an earlier work of Macpherson et al.[34]

From a theoretical perspective, it is clear that a knowledge of the full potential energy surface is needed for the improved application of a detailed statistical theory to this system, particularly at high temperatures, thereby avoiding the use of any interpolation parameter $\alpha$.

## 2. *Pressure-Dependent Rates*

The strengths and problems of studying the pressure-dependent recombination rates using a weak colliding gas is evident.[35] A brief preliminary report is given here of some calculations of Wagner et al.[35] on methyl radical recombination. Experimental rates for a discrete set of temperatures ranging from 295 to 1200 K were available as functions of Ar buffer gas concentration. These rates are plotted in Fig. 3 (with associated error bars, if available) versus the [Ar], which is seen to span one to three orders of magnitude, depending on the temperature studied. The theoretical analysis of the rates in Ref. 35 followed that in an earlier analysis of a different reaction,[36] except that a standard RRKM treatment of the transition state was replaced by the general transition state treatment for $k_{EJ}$ described in the previous section. Specifically, the $N_{EJ}(R)$ as given by Eq. (2.10) was evaluated by the method mentioned

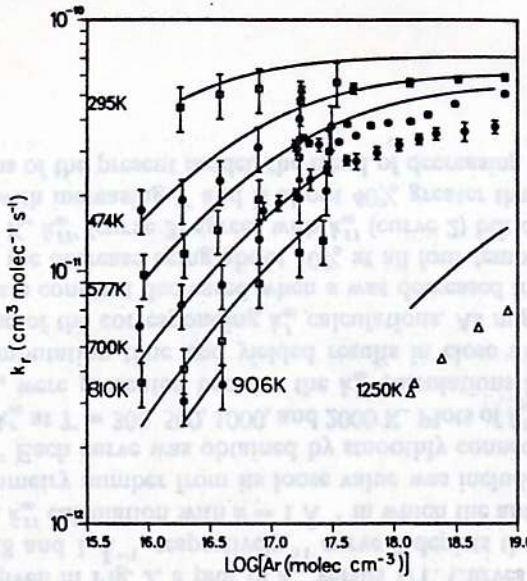


**Figure 3.** Logarithmic plot of the rate constant for $CH_3$ recombination versus argon buffer gas concentration at various temperatures. The solid curves are theoretical results obtained using generalized RRKM theory with $\alpha = 1$ Å$^{-1}$ and assuming an average energy transfer of $-190$ cm$^{-1}$ between buffer gas and metastable $C_2H_6$ per up and down collision. Experimental rates are indicated by various sysmbols with, in most cases, accompanying error bars; different symbols indicate rates obtained independently by different workers. Details are given in Ref. 35.

after Eq. (3.6) and employed for the sum of states at the transition state. A parameter $\langle \Delta E \rangle$ was varied from $\sim -175$ to $-300$ cm$^{-1}$ to obtain best agreement, $\langle \Delta E \rangle$ being the average energy transferred between buffer gas and metastable $C_2H_6$ per up and down collision. (The quantity $\langle \Delta E \rangle$ is related to an efficiency factor chosen so as to empirically mimic a master equation solution.[37]) The stabilization rate constant was taken to equal the product of the efficiency factor and a Lennard-Jones gas kinetic rate constant. For the value $\alpha = 1$ Å$^{-1}$ used earlier (Fig. 2), a value of $\langle \Delta E \rangle \simeq -190$ cm$^{-1}$ provided good agreement. The solid lines in Fig. 3 were computed with this value. Comparing theory and experiment on pressure effects with a weak collider, such as Ar, does introduce a new aspect, the unknown collision cross sections for the various deactivation and activation steps.

### 3. *Dissociation of Vibrationally Excited* $C_2H_6$

Growcock et al. determined the decomposition rate constant for vibrationally excited ethane produced by chemical activation, $C_2H_6^* \rightarrow 2CH_3$.[38] The

reported[38] excitation energy of $114.9 \pm 2$ kcal mol$^{-1}$ with respect to the zero-point energy of ethane corresponds, for the molecular parameters used in Ref. 11*c*, to an excess energy of $27.3 \pm 2$ kcal mol$^{-1}$ with respect to the zero-point energy of separated methyl radicals. Here, it was assumed that this excitation energy was deposited in internal degrees of freedom and the overall rotational energy of ethane was approximated by $E_J = J(J+1)/2I_{A,r}$ (in units of $\hbar = 1$) with a symmetric top moment of inertia $I_{A,r}$ defined in Ref. 11*b*. For $J$-dependent total energies $E - E_{zp} = 27.3 + E_J$ and various $J$'s, the $N_{EJ}(R_I^{\ddagger})$'s were determined. In each case $R_I^{\ddagger}$ was found to be $2.9 \pm 0.1$ Å. The calculated rate constants given by Eq. (2.1) were found to be $k_{EJ}$ (in $10^9$ sec$^{-1}$) = 4.6, 4.2, 4.4, 6.9, 14, and 33 for $J = 0$–125 in increments of 25.[11c] (At the lower $J$'s, $E_J$ at this $E$ is presumably too small to affect $k_{EJ}$.) These calculated $k_{EJ}$'s are consistent, for $J < 75$, with the reported[38] experimental value of $(4.6 \pm 1.2) \times 10^9$ sec$^{-1}$. The experimental $J$ distribution is not known. If $J$ had its thermally averaged value at room temperature (the temperature in the photolysis experiment[38] was not specified however), then the average $J$ would be about 25. In any event a $J$ distribution in which the dominant $J$'s are less than 75 is likely.

### B. $H_2O_2$ Dissociation

The unimolecular dissociation of isolated hydrogen peroxide in its ground electronic state

$$HOOH \rightarrow 2OH \tag{3.10}$$

has recently been studied experimentally[39–41] in a detailed manner. Statistical[39–41] theories have also been applied and classical trajectory[42] calculations have been made. In recent experiments the unimolecular decomposition of HOOH has been initiated by excitation of different OH stretching overtones (e.g., $5\nu_{OH}$ and $6\nu_{OH}$), and limited results for the partially deuterated species HOOD have also been obtained.[39–41] The yields of the different quantum states of the OH fragments were probed by time-resolved laser-induced fluorescence.

A vibrational–torsional potential model, in which the high-frequency OH vibration and the low-frequency torsional motion are adiabatically separated, was fit to the observed excitation spectra,[40] a model later modified to include the excitation of the O–O stretching vibration.[41] Peaks in the excitation spectrum were then assigned on the basis of this model (a main band involving pure OH stretching excitation, combination bands involving OH stretching excitation and torsional excitation, and hot bands for OH stretching excitation, in which the initial O–O vibration or torsional vibration was in an excited state).

In the work described subsequently, comparisons of experimental product

internal energy distributions to each other or to theoretical models, are given. Complementary information is provided by the rate of product formation, a quantity whose measurement is precluded in the experiments described herein by the 10 nsec time resolution. The study of the direct time-resolved picosecond measurements of HOOH decomposition and the rates of energy relaxation or reaction has recently been done by Zewail and co-workers.[43] Furthermore, experiments have been reported using Doppler spectroscopy and the laser-induced fluorescence technique to measure the translational energy distribution and the angular distribution of OH products.[44]

Results have been obtained by Rizzo et al.[39] for HOOH excited to the region of the fifth overtone ($6\nu_{OH}$) and by Ticich et al.[41a] for HOOH excited to the region of the fourth overtone ($5\nu_{OH}$). With six quanta in OH stretching, there is a minimum of 4.6 kcal mol$^{-1}$ of energy available for disposal in the products, when the molecule is in its lowest vibrational state initially. On the other hand, five quanta of OH stretching fall 12.9 kcal mol$^{-1}$ short of the O–O bond dissociation energy, so that only reactant molecules that initially have at least this much thermal energy can dissociate. Consequently, the resulting product distributions are expected to reflect the influence of threshold effects on the decay dynamics. For both the $6\nu_{OH}$ and $5\nu_{OH}$ cases, all excess energy is observed to appear in translation and rotation of the products; there is insufficient energy in the light quantum itself to produce a vibrationally excited OH. Measured product rotational distributions resulting from HOOH initially prepared in the main band ($6\nu_{OH}$) and in a combination band ($6\nu_{OH} + \nu_x$), where one quantum of torsional motion, $\nu_x$, is excited are compared in Fig. 4 for both the $R_1$ and $Q_1$ branches of the OH spectrum, $N$ denoting the rotational quantum number of an OH.

Statistical and experimental product distributions for excitation wavelengths in the region of HOOH ($5\nu_{OH}$) main and combination bands and in the region of the HOOH ($6\nu_{OH}$) main and combination bands are given in Fig. 5. The statistical product distributions calculated in Ref. 41 are based on two of the statistical models described in Section II: PST and the original SACM. (PST corresponds to the limiting SACM case of $\alpha \to \infty$, and in Ref. 41 the PST results were essentially identical to the SACM product distributions when $\alpha = 1.5$ Å$^{-1}$.) In the application of PST to this system it was found that the rather strong long-range attraction between OH fragments yielded centrifugal barriers at large separations and hence there were only small centrifugal barrier heights for physically reasonable values of the orbital angular momentum. The PST calculation was therefore found to be insensitive to the exact form of the long-range radial potential. The SACM and PST calculations included the initial distribution of the unexcited $H_2O_2$ and the effect of photoexcitation.[41a]

The experimental product distributions arising from decomposition of HOOH excited to the region of $5\nu_{OH}$ (Figs. 5*a* and 5*b*) are seen to be qualita-

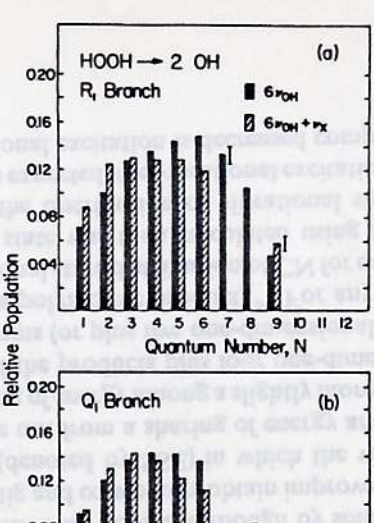


**Figure 4.** Relative rotational state distributions of OH products from overtone-vibration-induced unimolecular decomposition of HOOH. The solid bars are populations for excitation of the main local mode transition ($6\nu_{OH}$) and hatched bars are populations for excitation of the combination transition ($6\nu_{OH} + \nu_x$). The quantum number $N$ denotes the rotational OH angular momentum. Figures 4*a* and 4*b* show results obtained probing the $Q_1$ and $R_1$ branches, respectively, of OH. The error bars in Fig. 4(*a*) show the maximum range of values obtained and are typical of the uncertainties for all states. (Reproduced with permission from Ref. 39.)

tively different from the corresponding $6\nu_{OH}$ distributions (Figs. 5*c* and 5*d*). The $5\nu_{OH}$ distributions arise from decomposition of reactant states excited from the high-energy tail of the initial Boltzmann distribution, and many of these states therefore have energy near threshold. This is not the case for the $6\nu_{OH}$ decompositions. In parallel with new picosecond measurements of rates,[43] PST calculations are under way,[45] and calculations with the general transition state theory in Section II C are planned.

### C. NCNO Dissociation

Another unimolecular reaction that has been studied in great detail experimentally[46–49] is the collision-free decomposition of nitrosyl cyanide:

$$NCNO \rightarrow CN + NO. \tag{3.11}$$

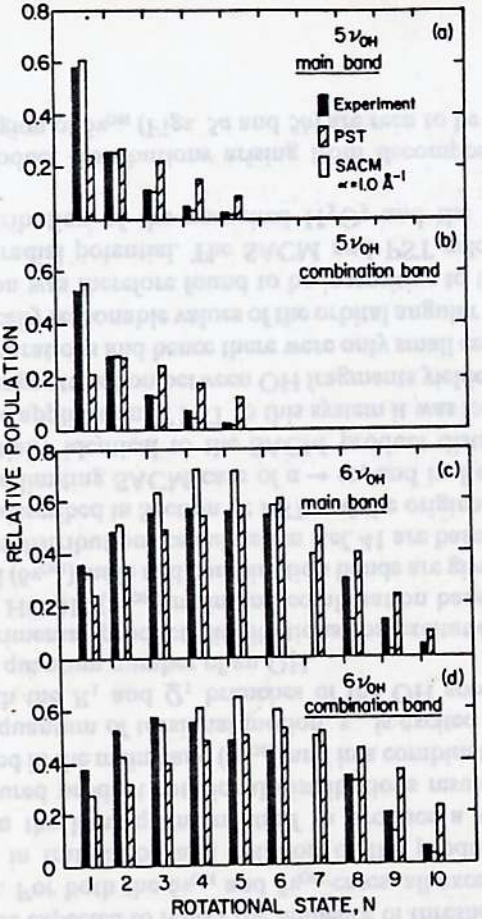


**Figure 5.** Comparison of the observed product rotational state distributions (solid bars) and the results of two statistical models: the statistical adiabatic channel model (SACM, open bars) and phase space theory (PST, hatched bars). The distributions are an average of those observed, or those calculated, at several excitation wavelengths in the region of (*a*) the $5\nu_{OH}$ main band, (*b*) the $5\nu_{OH}$ combination band, (*c*) the $6\nu_{OH}$ main band, and (*d*) the $6\nu_{OH}$ combination band of HOOH. (Reproduced with permission from Ref. 41.)

Using a pulsed free jet expansion the vibrational modes of the NCNO were in their ground states and, with He as a carrier gas, the rotational temperature of NCNO was about 2 K, corresponding to the symmetric top quantum states $J = 0$ to 6 and $K = 0$ to 1, where $J$ is the total rotational angular momentum and $K$ is its projection on the symmetry axis. The excitation of NCNO was

to a low-lying electronic state, which underwent internal conversion to the ground electronic state. The subsequent dissociation to CN and NO was slow on a rotational time scale.[49] The yields of the different rotational–vibrational quantum states of CN were monitored by laser-induced fluorescence. An accurate estimate of the dissociation energy $D_0$ of the NC–NO bond was obtained. Observation of the maximum value of $N''$, the rotational angular momentum of CN, permitted by having all available product energy, $E - D_0$, in CN rotation, provided evidence that the dissociation occurs on $S_0$ with no significant potential energy maximum in the exit channel.

Both CN and NO distributions were obtained, although the NO populations are considerably more difficult to measure.[49] In contrast to the $H_2O_2$ experiments in the previous section, it was possible to pump NCNO with sufficiently high-energy photons to obtain vibrationally excited CN or NO products, although the majority of experiments were performed with excitation energies below the thresholds for CN ($v'' = 1$) or NO ($v'' = 1$). Measured rotational distributions for CN and NO, as a function of their respective quantum numbers $N''$ and $J''$, are given in Fig. 6 (open circles) for three values of the photolysis wavelength, $\lambda_p$. The peaks in the photodissociation spectrum corresponding to the selected $\lambda_p$'s are indicated in the center panel of the figure. None of the three wavelengths was sufficiently short to result in vibrationally excited products. The spin-orbit splitting (123 $cm^{-1}$)[50] of the $X^2\Pi$ electronic state of NO resulted in separate rotational distributions for the $^2\Pi_{3/2}$ and $^2\Pi_{1/2}$ states at each excitation wavelength. There were no abrupt changes in the CN distributions with increasing $E - D_0$.[48]

PST is compared with the data in Fig. 6. When the energy available to products $E - D_0$ was below the product vibration excitational threshold, 1876 $cm^{-1}$ [NO at ($v'' = 1$)], the agreement of PST (solid circles) with the experimental rotational distributions in Fig. 6 was excellent. When $E - D_0$ was increased beyond 1876 $cm^{-1}$, the PST description of the rotational distributions became somewhat poorer, although by some standards still very good (e.g., Fig. 7). Wittig and co-workers obtain improved agreement by introducing a modification (denoted by SSE) in which the vibrational distribution was assumed to arise not from a sharing of energy among all coordinates (PST), but from a sharing of energy among a slightly more restricted number, namely, the vibrations of the products plus four one-dimensional translations in the case of two diatoms (or plus five one-dimensional translations in the case of a diatomic and a polyatomic product).[50] For any specified vibrational state of CN, the rotational state distribution of CN for each energetically accessible NO vibrational state was then calculated using PST, weighting each such distribution by the distribution of vibrational states of NO, calculated as above. In SSE, as expected, the vibrational excitation is now enhanced slightly and so the rotational excitation is decreased compared with PST. Below the

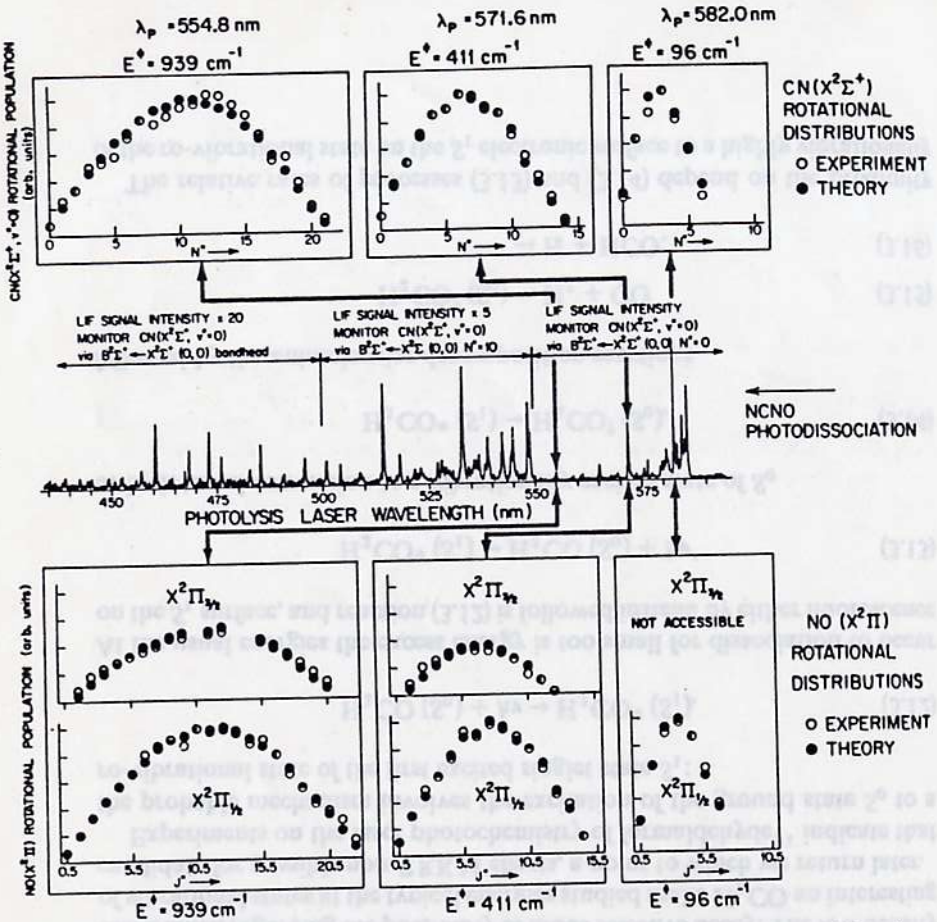


**Figure 6.** A composite view of the NO and CN data for the unimolecular decomposition of NCNO. The central trace shows the photodissociation spectrum of jet-cooled NCNO. The NO and CN rotational populations result from dissociation at the indicated absorption maxima. Experimental distributions for the CN rotational quantum number $N''$ and the NO rotational quantum number $J''$ are given as open circles in the upper and lower panels, respectively. The theoretical results are from PST. For a discussion of the calculated versus experimental NO spin-orbit population ratio see Ref. 49. (Reproduced with permission from Ref. 49.)

threshold for vibrational excitation, SSE and PST are identical. The results are given in Fig. 7, where PST and SSE are compared to the CN ($v'' = 0$) rotational distribution at $E - D_0 = 2348\ \text{cm}^{-1}$. Figure 8 gives a comparison of SSE and the data for both spin-orbit states of NO ($v'' = 1$) at the same excess energy. In order to compare theory with experiment it is necessary, in

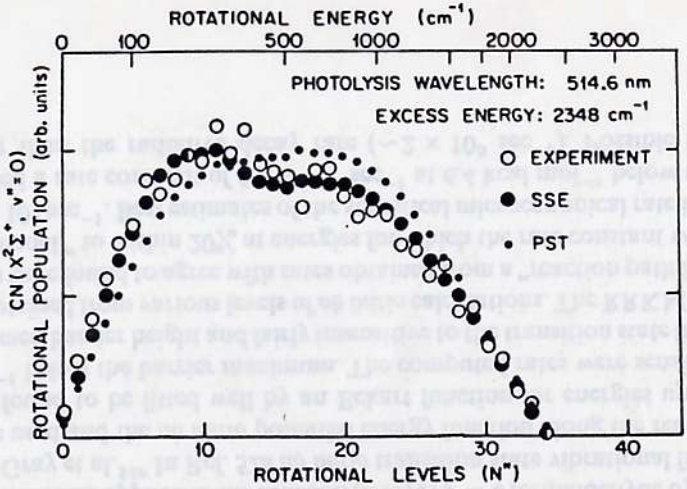


**Figure 7.** Comparison between experimental rotational distributions (open circles) and theoretical PST (small solid circles) and SSE (large solid circles) distributions for CN ($v'' = 0$) at $\lambda_p = 514.6$ nm and $E - D_0 = 2348$ cm$^{-1}$. (Reproduced with permission from Ref. 48.)

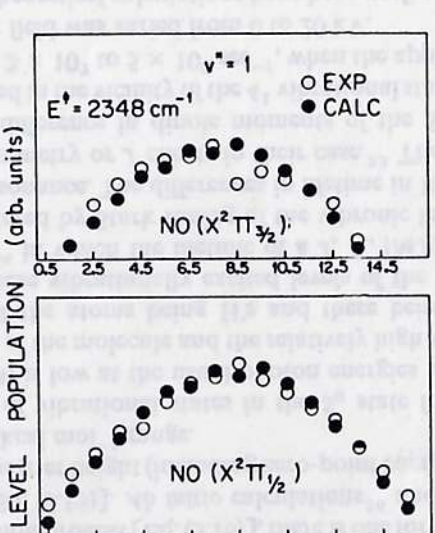


**Figure 8.** Experimental (open circles) and theoretical SSE (solid circles) rotational distributions for both spin-orbit states of NO ($v'' = 1$) with $E - D_0 = 2348$ cm$^{-1}$. See comment concerning the NO spin-orbit ratio in caption of Fig. 6. (Reproduced with permission from Ref. 49.)

principle, to average the PST and SSE distributions over the appropriate $P(E, J)$ distribution. Here only a few rotational states were populated initially ($T_{rot} \sim 2K; 0 \leq J \leq 6$) and, after photoexcitation, the ensemble of parent molecules had a rather narrow spread of $E$ and $J$ values. As the PST and SSE calculations were found to be fairly insensitive to the $J$ values over the range (0, 10), averaging was deemed unnecessary and so product distributions and product energy averages were determined only for $J = 5$. Further discussion of this system was given recently in a pair of articles.[50b] The RRKM plus adiabatic treatment in Section II C is expected to qualitatively produce the same effect as SSE, and it will be interesting to make a quantitative comparison with the data.

## D. $H_2CO$ Dissociation

Laser-induced formaldehyde dissociation has been intensively studied experimentally and theoretically in the last decade.[51-54] Detailed calculations of the potential energy surface have been reported and various studies have been undertaken regarding the possibility of mode selective decay. The low density of vibrational states at the typical energies studied make $H_2CO$ an interesting candidate for possible non-RRKM effects, a point to which we return later.

Experiments on the laser photochemistry of formaldehyde[51] indicate that the probable mechanism involves the excitation of the ground state $S_0$ to a ro-vibrational state of the first excited singlet state $S_1$:

$$H_2CO\,(S_0) + h\nu \rightarrow H_2CO^*\,(S_1). \tag{3.12}$$

At the usual energies the excess energy is too small for dissociation to occur on the $S_1$ surface, and reaction (3.12) is followed instead by either fluorescence

$$H_2CO^*\,(S_1) \rightarrow H_2CO\,(S_0) + h\nu' \tag{3.13}$$

or by internal conversion to a vibrationally excited state of $S_0$

$$H_2CO^*\,(S_1) \rightarrow H_2CO^\dagger\,(S_0), \tag{3.14}$$

followed by the unimolecular decomposition reactions

$$H_2CO^\dagger\,(S_0) \rightarrow H_2 + CO \tag{3.15}$$

$$\rightarrow H + HCO. \tag{3.16}$$

The relative rates of processes (3.13) and (3.14) depend on the proximity of the ro-vibrational state on the $S_1$ electronic surface to a highly vibrationally

excited state on $S_0$. The radiationless decay rate [Eq. (3.14)] will be maximized when two vibronic states of $S_0$ and $S_1$ are in resonance, a condition exploited in recent Stark tuning experiments.[53,54]

The threshold for decay to radical products [Eq. (3.16)] is higher than that for molecular products [Eq. (3.15)]. At excitation energies sufficiently close to the origin of the $S_0 \rightarrow S_1$ transition only molecular products are observed and Eq. (3.16) becomes more important with increasing excitation energy.[55] Whereas there is presumably no barrier maximum for the dissociation in the simple bond fission process [Eq. (3.16)], there is one for the molecular elimination channel [Eq. (3.15)]. *Ab initio* calculations[56] and a fit to experimental data[54] put the barrier height (including zero-point energies) for reaction (3.15) in the $\sim$80–90 kcal mol$^{-1}$ range.

The density of vibrational states in the $S_0$ state formed in the internal conversion (3.14) is low at the usual photon energies used in (3.12), because of the smallness of the molecule and the relatively high values of the vibration frequencies, half the atoms being H's and there being a C=O bond. The sparseness of these vibrationally excited levels of the $S_0$ state is evident in recent work[53,54] in which the lifetime of a $J$, $K$, $|M|$-resolved $S_1$ state was considerably altered by Stark tuning of the vibronic levels of the two states in and out of resonance. The differences in lifetime in Ref. 53 were found not to be due to symmetry or $J$ effects in their case.[53] The tuning was possible because of the difference in dipole moments of the $S_0$ and $S_1$ states. For $D_2CO(S_1)$ excited in the vicinity of the $4^1$ vibrational state, decay rates ranged irregularly from $2 \times 10^7$ to $5 \times 10^8$ sec$^{-1}$, when the applied voltage responsible for the Stark field was varied from 0 to 20 kV.

A variety of theoretical calculations have been performed, including classical trajectory studies of chaotic versus quasiperiodic motion.[57] Approximate tunneling corrections within the framework of RRKM (i.e., microcanonical transition state) theory have been used, in which the one-dimensional barrier along the reaction coordinate was represented by the generalized Eckart potential and applied to the reaction (3.15) of $J = 0$ formaldehyde by Miller[52a] and Gray et al.[52b] In Ref. 52*a* *ab initio* transition state vibrational frequencies were used and the *ab initio* potential energy function along the reaction path was found to be fitted well by an Eckart function for energies up to 8 kcal mol$^{-1}$ below the barrier maximum. The computed rates were sensitive to the assumed barrier height and fairly insensitive to the transition state frequencies as obtained from various levels of *ab initio* calculations. The RRKM tunneling rates were found to agree with rates obtained from a "reaction path Hamiltonian model," to within 20% at energies for which the rate constant was greater than $10^5$ sec$^{-1}$. Best estimates of the statistical microcanonical rate in Ref. 52*b* yielded a rate constant of $5.9 \times 10^6$ sec$^{-1}$ at 6.4 kcal mol$^{-1}$ below threshold, faster than the radiative decay rate ($\sim 2 \times 10^5$ sec$^{-1}$). Possible symmetry

effects for states symmetrical and antisymmetrical with respect to the $H_2CO$ plane were also examined, and an RRKM plus tunneling model[58a] was applied to each irreducible representation to obtain $J = 0$ microcanonical rate constants for formaldehyde decomposition. A factor of $\sim 20$ difference between them at $J = 0$ was predicted in the tunneling region, which became a factor of 2 at 5–6 kcal $mol^{-1}$ above threshold, and unity as $E \to \infty$. Results for nonzero total angular momentum revealed a diminished symmetry specificity for $J > 0$.[58b]

Troe has calculated $k_{EJ}$ for the molecular elimination channel (3.15),[59] using an RRKM plus tunneling model, namely, a model analogous to that in Ref. 57 but with slightly different molecular parameters and including approximate anharmonicity correction factors based on a coupled Morse oscillator model. Using a simplified SACM for (3.16), the calculations led him to suggest a channel switching of the two mechanisms at $J \sim 35$, channel (3.15) being more important than (3.16) when $J < 35$, this being reversed for $J > 35$.

## IV. DYNAMICAL ASPECTS AND STATISTICAL BEHAVIOR

In the preceding sections several statistical approaches for calculating reaction rates and distributions of quantum states were described and illustrated using recent studies. We conclude with some remarks on the dynamical aspects leading to and creating deviations from statistical theories.

A dynamical basis for statistical theories is a matter of much current interest.[60] We consider first the case where the vibrational or really vibrational–rotational quantum states of the molecule are those of a bound system, that is, where there is no dissociation. The Hamiltonian $H$ can be regarded as a perturbation (parameter $\lambda$) from some integrable Hamiltonian $H_0(\lambda = 0)$, for example, from a collection of normal modes or Morse oscillator modes to, say, $\lambda = 1$. The eigenvalues in $H_0$ occur in sequences, sequences which can have spacings slowly varying with the quantum numbers (as in a collection of Morse oscillators, for example).[60a] If the spacings of the eigenvalues are sufficiently large, the perturbation from $H_0$ to $H$ produces no avoided crossings of the eigenvalues in the vicinity of $\lambda = 1$ and so the wavefunctions of $H$ at $\lambda = 1$, like those of $H_0$, can be expected to be "mode selective,"[60a,61] and the eigenvalues can be expected to occur in sets of regular sequences.[60a] If, on the other hand, the levels are sufficiently closely spaced, they may approach each other closely at $\lambda = 1$, and one obtains then a "mixing" of states. If a particular such level participates in many such avoided crossings simultaneously (overlapping avoided crossings[62]), the wavefunction takes on a statistical character (highly irregular nodal patterns), and its behavior will differ only randomly from that of nearby states.[63] Such then are two limiting dynamical pictures of the vibrational eigenstates of $H$.

If now the states of $H$ are coupled to a continuum via a nuclear tunneling through a potential energy barrier, the same two limiting pictures as given previously, can be expected to occur, but now each state of $H$ is broadened by the coupling to the continuum. A case in point may be $H_2CO$, whose states in the tunneling regime showed, as noted earlier, considerable differences.

The next case in increasing complexity is where the predissociative states of $H$ do not involve a nuclear tunneling. Here, a suitable choice for an $H_0$ may not be evident.[64] (One possibility is for $H_0$ to consist of a Morse oscillator for the dissociating mode and normal modes for each fragment, but this would need to be supplemented by coupled $R$-dependent hindered rotations of the fragments.) Indeed, the difficulty in finding such an $H_0$ may be consistent with a considerable "mixing" of the states as a whole in such systems. As before, the more widely spaced the states, the less the extent of "mixing" and the greater the opportunity for observing a mode-selective behavior.

Regardless of whether the $H$ has "mode-selective" or "highly mixed" eigenstates, the excitation process can involve, when the eigenstates are sufficiently closely spaced, the formation of a wavepacket of states: Many states whose energies lie within the width of the laser pulse may be optically active. An example of mixed and mode-selective behavior is seen in recent work on infrared fluorescence after excitation by a single infrared photon.[65] Here, depending on the number of coordinates, the infrared excitation of a molecule by a single vibrational quantum yielded infrared fluorescence from many parts of the molecule, when the molecule was sufficiently large. Examples of "mode selectivity" in vibrational states, that is, nonstatistical behavior, include the observation of vibrational quantum beats in some organic molecules at low energies,[66] the behavior of some van der Waals' complexes,[67] and perhaps the studies in $H_2CO$ mentioned earlier.[53,54] Experiments on "mode selectivity" in the tunneling and nontunneling regimes, for molecules of different complexity is clearly of considerable interest in defining some limitations of statistical theoreies.

In a concluding comment we recall some ideas on a topic that has frequently arisen in discussions of dynamical and statistical behavior, namely, the relation between what was previously termed "highly mixed quantum states" and "chaos." As noted elsewhere,[68] classical chaos is expected to imply some corresponding behavior in the quantum case, such as "highly mixed states," but only when the classical chaos is, on a phase-space scale, large compared with $h$.[69] A more detailed discussion, based on Chirikov's idea for the origin of classical chaos (overlapping resonances) and the connection between classical resonances and quantum-mechanical avoided crossings, has been given elsewhere.[62,69]

It may also be recalled that there are two types of "global states": In particular, one can have states that, owing to the presence of an isolated

quantum-mechanical resonance, may have a delocalized character. Such states will, when projected onto a set of localized basis set states, have many components. Nevertheless, the state may still be regular, that is, not participate in overlapping avoided crossings and be a member of a set of states which has a high regularity in its eigenvalue sequences. It was shown elsewhere[70] that the "global states" of Nordholm and Rice, for example, were of this type.[71] There is also another type of global state, namely, a state that is delocalized by virtue of being involved in many overlapping avoided crossings. These two types of global states will exhibit some differences in properties, as well as some similarities. Detailed experimental pump-probe measurements are only now just beginning to unravel the nature of the vibrational and rotational states of vibrationally excited molecules.

## Acknowledgment

It is a pleasure to acknowledge the support of this research by the Natural Sciences and Engineering Research Council of Canada (D.M.W.) and by the National Science Foundation (R.A.M.).

## References

1. R. A. Marcus, W. L. Hase, and K. N. Swamy, *J. Phys. Chem.* **88**, 6717 (1984).
2. R. A. Marcus, *J. Chem. Phys.* **85**, 5035 (1986).
3. For example, P. J. Robinson and K. A. Holbrook, *Unimolecular Reactions*. Wiley, New York, 1972. W. Forst, *Theory of Unimolecular Reactions*. Academic, New York, 1973. A. B. Callear, in *Comprehensive Chemical Kinetics* (C. H. Bamford and C. F. H. Tipper, eds.) Elsevier, New York, 1983, Vol. 24, Chap. 4.
4. For example, I. Oref and B. S. Rabinovitch, *Acc. Chem. Res* **12**, 166 (1979), I. W. M. Smith, *Kinetics and Dynamics of Elementary Gas Reaction Rates*. Pergamon Oxford, 1966, Chap. 3.
5. There is a large body of literature on these newer developments, for example, W. B. Miller, S. A. Safron, and D. R. Herschbach, *J. Chem. Phys.* **56**, 3581 (1972); J. M. Farrar and Y. T. Lee, *ACS Symp. Ser.* **66**, 191 (1978); S. Stolte, A. E. Proctor, W. M. Pope, and R. B. Bernstein, *J. Chem. Phys.* **66**, 3468 (1977); R. B. Bernstein, *Chemical Dynamics via Molecular Beam and Laser Techniques*. Oxford University Presss, 1982; K. V. Reddy and M. J. Berry, *Chem. Phys. Lett.* **66**, 223 (1979); J. W. Hudgens and J. D. McDonald, *J. Chem. Phys.* **76**, 173 (1982), F. F. Crim, *Annu. Rev. Phys. Chem.* **35**, 657 (1984); K. Rynefors, P. A. Elofson, and L. Holmlid, *Chem. Phys.* **90**, 347 (1984), N. Scherer, F. E. Doany, A. H. Zewail, and J. Perry, *J. Chem. Phys.* **84**, 1932 (1986), and references cited in these articles. Many more recent examples include those in various articles in *J. Phys. Chem.* **90**, No. 16 (1986), such as in R. B. Bernstein and A. H. Zewail, p. 3467; D. L. Snavely, R. N. Zare, J. A. Miller, and D. W. Chandler, p. 3544; A. M. Wodtke, E. J. Hintsa, and Y. T. Lee, p. 3549; S. Olesik, T. Baer, and J. C. Morrow, p. 3563; H.-S. Kim, M. F. Jarrold, and M. T. Bowers, p. 3584.
6. (*a*) R. A. Marcus, *J. Chem. Phys.* **20**, 359 (1952); R. A. Marcus and O. K. Rice, *J. Phys. Colloid. Chem.* **55**, 894 (1951); (*b*) R. A. Marcus, *J. Chem. Phys.* **43**, 2658 (1965); **52**, 1018 (1970).
7. E. Gorin, *Acta Physicockim. U.R.S.S.* **9**, 691 (1938).
8. (*a*) S. A. Safron, N. D. Weinstein, D. R. Herschbach, and J. C. Tully, *Chem. Phys. Lett.* **12**, 564 (1972); (*b*) D. M. Wardlaw, Ph.D. dissertation, University of Toronto, 1982.
9. R. A. Marcus, *J. Chem. Phys.* **62**, 1372 (1975); G. Worry and R. A. Marcus, *J. Chem. Phys.* **67**, 1636 (1977).

10. Cf. R. A. Marcus, *J. Chem. Phys.* **45**, 2630 (1966). This paper contains this criterion (p. 2635), but mistakenly ascribes it to Bunker, who actually uses, instead, a minimized density of states criterion [D. L. Bunker and M. Pattengill, *J. Chem. Phys.* **48**, 772 (1968)]. This minimum number of states criterion has been used by various authors, for example, W. L. Hase, *J. Chem. Phys.* **57**, 730 (1972); **64**, 2442 (1976); M. Quack and J. Troe (Ref. 21); B. C. Garrett and D. G. Truhlar, *J. Chem. Phys.* **70**, 1593 (1979). The transition state theory utilizing it is now frequently termed microcanonical variational transition state theory ($\mu$VTST). A recent review of $\mu$VTST and of canonical VTST is given in D. G. Truhlar and B. C. Garrett, *Ann. Rev. Phys. Chem.* **35**, 159 (1984).
11. D. M. Wardlaw and R. A. Marcus, (*a*) *Chem. Phys. Lett.* **110**, 230 (1984), (*b*) *J. Chem. Phys.* **83**, 3462 (1985), (*c*) *J. Phys. Chem.* **90**, 5383 (1986). The notation in the present paper is that employed in (*c*). There are several minor errors in (*c*): the factor $(2J + 1)$ should be deleted from Eq. (I.3); in Table V, the heading for the fourth column should be $N_{E,J}(R^{\ddagger})\sigma_i/(2J + 1)$, with $\sigma_i$ as defined in the text; in Table IX, the headings for the second and third columns should be $[N_E \pm \sigma^{MC}]\sigma_i/10^{18}$ and $[N_E^A \pm \sigma_A^{MC}]\sigma_i/10^{18}$, respectively; in Eqs. (IV.1), (IV.3), and (IV.4), the quantity $g_e$ should be in the numerator rather than in the denominator.
12. P. Pechukas and J. C. Light, *J. Chem. Phys.* **42**, 3281 (1965); P. Pechukas, J. C. Light, and C. Rankin, *J. Chem. Phys.* **44**, 794 (1966).
13. For example, C. J. Cobos and J. Troe, *J. Chem. Phys.* **83**, 1010 (1985); S. W. Benson, *Can. J. Chem.* **61**, 881 (1983); W. L. Hase and R. J. Duchovic, *J. Chem. Phys.* **83**, 3448 (1985), and references cited therein.
14. (*a*) E. Wigner, *J. Chem. Phys.* **5**, 720 (1937); (*b*) *Trans. Faraday Soc.* **34**, 29 (1938); (*c*) J. C. Keck, *Adv. Chem. Phys.* **13**, 85 (1967).
15. R. A. Marcus, *J. Chem. Phys.* **43**, 1598 (1965).
16. J. O. Hirschfelder and E. Wigner, *J. Chem. Phys.* **7**, 616 (1939).
17. For example, M. A. Eliason and J. O. Hirschfelder, *J. Chem. Phys.* **30**, 1426 (1959); L. Hofacker, *Z. Naturforsch.* **18a**, 607 (1963); R. A. Marcus. Ref. 15; R. A. Marcus, *J. Chem. Phys.* **45**, 4493, (1966); **45**, 4500 (1966). Additional references are given in M. M. Kreevoy and D. G. Truhlar, in *Investigations of Rates and Mechanisms of Reactions*. (C. F. Bernasconi, ed.). Wiley, New York, 1986, Vol 6, Part 1, p. 13.
18. M. Quack and J. Troe, *Ber. Bunsenges. Phys. Chem.* **78**, 240 (1974).
19. (*a*) Another interpolation function, $\frac{1}{3}(2g + g^2)$, has been reported to reproduce satisfactorily $R$-dependent eigenvalues for a particular 1$D$-hindered rotor [M. Quack, *J. Phys Chem.* **83**, 150 (1979)]. The $k_{E,J}$ in one study changed by a factor of 2, compared with the use of (2.13).[11b] (*b*) Various views on the use of an interpolation function to describe a potential energy surface are given in R. J. Duchovic, W. L. Hase, and H. B. Schlegel, *J. Phys. Chem.* **88**, 1339 (1984); F. B. Brown and D. G. Truhlar, *Chem. Phys. Lett.* **113**, 441 (1985); S. Peyerimhoff, M. Lewerenz, and M. Quack, *Chem. Phys. Lett.* **109**, 563 (1984).
20. J. Troe, *J. Phys. Chem.* **88**, 4375 (1984); C. J. Cobos and J. Troe, Ref. 13.
21. M. Quack and J. Troe, *Ber. Bunsenges. Phys. Chem.* **81**, 329 (1977); J. Troe, *J. Chem. Phys.* **79**, 6017 (1983), and references cited therein.
22. M. Quack and J. Troe, *Ber. Bunsenges. Phys. Chem.* **79**, 469 (1975).
23. W. J. Chesnavich, L. Bass, T. Su, and M. T. Bowers, *J. Chem. Phys.* **74**, 2228 (1981); M. F. Jarrold, L. M. Bass, P. R. Kemper, P. A. M. van Koppen, and M. T. Bowers, *J. Chem. Phys.* **78**, 3756 (1983); M. T. Bowers, M. F. Jarrold, W. Wagner-Redeker, P. R. Kemper, and L. M. Bass, *Faraday Disscuss. Chem. Soc.* **75**, 57 (1983); S. Olesik, T. Baer, and J. C. Morrow, Ref. 5; H.-S. Kim, M. F. Jarrold, and M. T. Bowers, Ref. 5
24. J. A. Dodd, D. M. Golden, and J. I. Brauman, *J. Chem. Phys.* **80**, 1894 (1984); D. G. Truhlar, *J. Chem. Phys.* **82**, 2166 (1985); W. J. Chesnavich and M. T. Bowers, *J. Chem. Phys.* **82**, 2168 (1985); K. N. Swamy and W. L. Hase, *J. Chem. Phys.* **77**, 3011 (1982); S. L. Mondro, S. Vande Linde, and W. L. Hase, *J. Chem. Phys.* **84**, 3783 (1986).

25. D. B. Olson and W. C. Gardiner, *J. Phys. Chem.* 83, 922 (1979), and references cited therein.
26. D. L. Baulch and J. Duxbury, *J. Combust. Flame* 37, 313 (1980), and references cited therein.
27. W. L. Hase, *J. Chem. Phys.* 64, 2442 (1976).
28. For example, R. A. Marcus, *J. Chem. Phys.* 43, 2658 (1965); Eq. (3.3) is a straightforward adaptation of the unimolecular case treated in this reference.
29. For example, see R. E. Weston and H. A. Schwarz, *Chemical Kinetics.* Prentice-Hall, Englewood Cliffs, NJ, 1972.
30. M. Abramowitz and I. Stegun, *Handbook of Mathematical Functions.* Dover, New York, 1965; the Laguerre quadrature is given on p. 890.
31. Calculations with $\alpha = 0.8$ Å$^{-1}$ (curve 1) were performed, in addition to $\alpha = 1$ Å$^{-1}$, because the choice for the potential energy surface interpolation parameter although reasonable is somewhat arbitrary. Hase[27] used $\alpha = 0.82$ Å$^{-1}$, based on a fit of ethane decomposition rates to the experimental data.
32. S. W. Benson, in Ref. 13.
33. M. T. Macpherson, M. J. Pilling, and M. J. C. Smith, *J. Phys. Chem.* 89, 2268 (1985).
34. M. T. Macpherson, M. J. Pilling, and M. J. C. Smith, *Chem. Phys. Lett.* 94, 430 (1983).
35. A. F. Wagner and D. M. Wardlaw, submitted to *J. Phys. Chem.*
36. L. B. Harding and A. F. Wagner, *XXI International Symposium on Combustion* (to be published).
37. J. Troe, *J. Phys. Chem.* 87, 1800 (1983).
38. F. B. Growcock, W. L. Hase, and J. W. Simons, *Int. J. Chem. Kinet.* 5, 77 (1973).
39. T. R. Rizzo, C. C. Hayden, and F. F. Crim, *J. Chem. Phys.* 81, 4501 (1984).
40. H.-R. Dubal and F. F. Crim, *J. Chem. Phys.* 83, 3863 (1985).
41. (*a*) T. M. Ticih, T. R. Rizzo, H.-R. Dubal, and F. F. Crim, *J. Chem. Phys.* 84, 1508 (1986). (*b*) See also L. J. Butler, T. M. Ticich, M. D. Likar, and F. Crim, *J. Chem. Phys.* 85, 2331 (1986).
42. T. Uzer, J. T. Hynes, and W. P. Reinhardt, *Chem. Phys. Lett.* 117, 600 (1985); *J. Chem. Phys.* 85, 5791 (1986); R. Bersohn and M. Shapiro, *J. Chem. Phys.* 85, 1396 (1986).
43. N. F. Scherer, F. E. Doany, A. H. Zewail, and J. W. Perry, in Ref. 5.
44. S. Klee, K.-H. Gericke, and F. J. Comes, *J. Chem. Phys.* 85, 40 (1986).
45. N. F. Scherer and A. H. Zewail (private communication).
46. I. Nadler, H. Reisler, M. Noble, and C. Wittig, *Chem. Phys. Lett.* 108, 115 (1984).
47. M. Noble, I. Nadler, H. Reisler, and C. Wittig, *J. Chem. Phys.* 81, 4333 (1984).
48. I. Nadler, M. Noble, H. Reisler, and C. Wittig, *J. Chem. Phys.* 82, 2608 (1985).
49. C. X. W. Qian, M. Noble, I. Nadler, H. Reisler, and C. Wittig, *J. Chem. Phys.* 83, 5573 (1985).
50. (*a*) C. Wittig, I. Nadler, H. Reisler, M. Noble, J. Catanzarite, and G. Radhakrishnan, *J. Chem. Phys.* 83, 5581 (1985); (*b*) C. Wittig, I. Nadler, H. Reisler, M. Noble, J. Catanzarite, and G. Radhakrishnan *J. Chem. Phys.* 85, 1710 (1986); J. Troe, *J. Chem. Phys.* 85, 1708 (1986).
51. C. B. Moore and J. C. Weisshaar, *Annu. Rev. Phys. Chem.* 34, 525 (1983), and references cited therein.
52. (*a*) W. H. Miller, *J. Am. Chem. Soc.* 101, 6810 (1979); (*b*) S. K. Gray, W. H. Miller, Y. Yamaguchi, and H. F. Schaefer, *J. Am. Chem. Soc.* 103, 1900 (1981).
53. H.-L. Dai, R. W. Field, and J. L. Kinsey, *J. Chem. Phys.* 82, 1606 (1985).
54. D. R. Guyer, W. F. Polik, and C. B. Moore, *J. Chem. Phys.* 84, 6519, (1986).
55. Th. Just, *Symp (Int.) Combust.* [Proc.], 17th, 584 (1979); J. H. Clark, C. B. Moore and N. S. Nogar, *J. Chem. Phys.* 70, 5135 (1979).
56. J. D. Goddard, Y. Yamaguchi, and H. F. Schaefer, *J. Chem. Phys.* 75, 3459 (1981); M. J. Frisch, R. Krishnan, and J. A. Pople, *J. Phys. Chem.* 85, 1467 (1981); M. Dupuis, W. A. Lester, B. H. Lengsfield, and B. Lui, *J. Chem. Phys.* 79, 6167 (1983).
57. K. N. Swamy and W. L. Hase, *Chem. Phys. Lett.* 92, 371 (1982); S. K. Gray and M. S. Child, *Mol. Phys.* 53, 961 (1984).

58. (*a*). W. H. Miller, *J. Am. Chem. Soc.* **105**, 216 (1983); R. A. Marcus, *J. Chem. Phys.* **45**, 2138 (1966); (*b*) W. H. Miller, *J. Phys. Chem.* **87**, 2731 (1983); see also B. A. Waite, S. K. Gray, and W. H. Miller, *J. Chem. Phys.* **78**, 259 (1983).
59. J. Troe, *J. Phys. Chem.* **88**, 4375 (1984).
60. (*a*) D. W. Noid, M. L. Koszykowski, and R. A. Marcus, *Annu. Rev. Phys. Chem.* **32**, 267 (1981); (*b*) F. H. Mies, *J. Chem. Phys.* **51**, 787 (1969); **51**, 798 (1969); K. G. Kay, *J. Chem. Phys.* **65**, 3813 (1976); recent articles in *J. Phys. Chem.* **90**, No. 16 (1986), such as S. K. Gray, S. A. Rice, and M. J. Davis, p. 3470; J. M. Bowman, p. 3492; R. S. Dumont and P. Brumer, p. 3509; K. N. Swamy, W. L. Hase, B. C. Garrett, C. W. McCurdy, and J. F. McNutt, p. 3517; R. C. Brown and R. E. Wyatt, p. 3590; M. S. Child, p. 3595; P. Pechukas, p. 3603; E. Pollak, p. 3619.
61. Examples of mode selectivity in calculations appear in Ref. 58 and in several of the articles in Ref. 60.
62. R. A. Marcus, in *Horizons in Quantum Chemistry*. (K. Fukui and B. Pullman, eds.). Reidel, Dordrecht, 1980, p. 107; *Ann. N. Y. Acad. Sci.* **357**, 169 (1980); *Faraday Discuss. Chem. Soc.* **75**, 103 (1983).
63. For example, R. A. Marcus, Extended Abstracts, 27th Annual Conference on Mass Spectrometry and Allied Topics, Seattle, WA (Am. Soc. Mass Spectroscopy, 1979), p. 568; V. Buch, R. B. Gerber, and M. A. Ratner, *J. Chem. Phys.* **81**, 3393 (1984); M. Feingold, N. Moiseyev, and A. Peres, *Chem. Phys. Lett.* **117**, 344 (1985).
64. Recent examples of choices of a Hamiltonian for dissociation, isomerization, or intramolecular energy transfer include those in Z. Bacic, R. B. Gerber, and M. A Ratner, *J. Phys. Chem.* **90**, 3606 (1986); in S. K. Gray, W. H. Miller, Y. Yamaguchi, and H. F. Schaefer, *J. Chem. Phys.* **73**, 2733 (1980); and in R. D. Levine and J. L. Kinsey, *J. Phys. Chem.* **90**, 3653 (1986).
65. G. M. Stewart and J. D. McDonald, *J. Chem. Phys.* **78**, 3907 (1983); G. M. Stewart, M. D. Ensminger, T. J. Kulp, R. S. Ruoff, and J. D. McDonald, *J. Chem. Phys.* **79**, 3190 (1983); T. J. Kulp, H. L. Kim, and J. D. McDonald, *J. Chem. Phys.* **85**, 211 (1986).
66. W. R. Lambert, P. M. Felker, and A. H. Zewail, *J. Chem. Phys.* **75**, 5958 (1981); **81**, 2217 (1984).
67. D. H. Levy, *Annu. Rev. Phys. Chem.* **31**, 197 (1980); K. W. Butz, D. L. Catlett, G. E. Ewing, D. Krajnovich, and C. S. Parmenter, *J. Phys. Chem.* **90**, 3533 (1986).
68. A brief summary and references are given in R. A. Marcus, in *Chaotic Behavior in Quantum Systems* (G. Casati, ed.). Plenum, New York, 1985, p. 293.
69. An example where a system showed classical chaos but regular eigenvalue sequences is given in D. W. Noid, M. L. Koszykowski, M. Tabor, and R. A. Marcus, *J. Chem. Phys.* **73**, 391 (1980).
70. D. W. Noid and R. A. Marcus, *J. Chem. Phys.* **67**, 559 (1977). The regularity of the eigenvalue sequences was demonstrated in Ref. 69.
71. K. S. J. Nordholm and S. A. Rice, *J. Chem. Phys.* **61**, 203 (1974); **61**, 768 (1974); **62**, 157 (1975).